Biomedical Optics EXPRESS

A compact Airy beam light sheet microscope with a tilted cylindrical lens

Zhengyi Yang,[1] Martynas Prokopas,[1] Jonathan Nylk,[1,2] Clara Coll-Lladó,[3] Frank J. Gunn-Moore,[2] David E. K. Ferrier,[3] Tom Vettenburg,[1] and Kishan Dholakia[1,*]

[1]*SUPA, School of Physics and Astronomy, University of St Andrews, North Haugh, St Andrews, KY16 9SS, UK*
[2]*School of Biology, Medical and Biological Sciences Building, University of St Andrews, North Haugh, St Andrews, KY16 9TF, UK*
[3]*The Scottish Oceans Institute, Gatty Marine Laboratory, School of Biology, University of St Andrews, East Sands, St Andrews, KY16 8LB, UK*
kd1@st-andrews.ac.uk

Abstract: Light-sheet imaging is rapidly gaining importance for imaging intact biological specimens. Many of the latest innovations rely on the propagation-invariant Bessel or Airy beams to form an extended light sheet to provide high resolution across a large field of view. Shaping light to realize propagation-invariant beams often relies on complex programming of spatial light modulators or specialized, custom made, optical elements. Here we present a straightforward and low-cost modification to the traditional light-sheet setup, based on the open-access light-sheet microscope OpenSPIM, to achieve Airy light-sheet illumination. This brings wide field single-photon light-sheet imaging to a broader range of endusers. Fluorescent microspheres embedded in agarose and a zebrafish larva were imaged to demonstrate how such a microscope can have a minimal footprint and cost without compromising on imaging quality.

OCIS codes: (170.0170) Medical optics and biotechnology; (180.6900) Three-dimensional microscopy; (140.3300) Laser beam shaping; (220.1000) Aberration compensation; (070.0070) Fourier optics and signal processing; (110.0180) Microscopy; (110.1758) Computational imaging; (110.4850) Optical transfer functions; (110.7348) Wavefront encoding.

References and links

1. J. Huisken, J. Swoger, F. Del Bene, J. Wittbrodt, and E. H. K. Stelzer, "Optical sectioning deep inside live embryos by selective plane illumination microscopy," Science **305**(5686), 1007–1009 (2004).
2. C. J. Engelbrecht and E. H. K. Stelzer, "Resolution enhancement in a light-sheet-based microscope (SPIM)," Opt. Lett. **31**(10), 1477–1479 (2006).
3. J. Huisken and D. Y. R. Stainier, "Even fluorescence excitation by multidirectional selective plane illumination microscopy (mSPIM)," Opt. Lett. **32**(17), 2608–2610 (2007).
4. R. Tomer, K. Khairy, F. Amat, and P. J. Keller, "Quantitative high-speed imaging of entire developing embryos with simultaneous multiview light-sheet microscopy," Nat. Methods **9**, 755–763 (2012).
5. J. A. N. Buytaert and J. J. J. Dirckx, "Design and quantitative resolution measurements of an optical virtual sectioning three-dimensional imaging technique for biomedical specimens, featuring two-micrometer slicing resolution," J. Biomed. Opt. **12**(1), 014039 (2007).
6. T. A. Planchon, L. Gao, D. E. Milkie, M. W. Davidson, J. A. Galbraith, C. G. Galbraith, and E. Betzig, "Rapid three-dimensional isotropic imaging of living cells using Bessel beam plane illumination," Nat. Methods **8**, 417–423 (2011).

#214434 - $15.00 USD Received 24 Jun 2014; revised 18 Aug 2014; accepted 22 Aug 2014; published 5 Sep 2014

7. O. E. Olarte, J. Licea-Rodriguez, J. A. Palero, E. J. Gualda, D. Artigas, J. Mayer, J. Swoger, J. Sharpe, I. RochaMendoza, R. Rangel-Rojo, and P. Loza-Alvarez, "Image formation by linear and nonlinear digital scanned lightsheet fluorescence microscopy with Gaussian and Bessel beam profiles," Biomed. Opt. Express **3**(7), 1492–1505 (2012).
8. L. Gao, L. Shao, C. D. Higgins, J. S. Poulton, M. Peifer, M. W. Davidson, X. Wu, B. Goldstein, and E. Betzig, "Noninvasive imaging beyond the diffraction limit of 3D dynamics in thickly fluorescent specimens," Cell **151**(6), 1370–1385 (2012).
9. T. Vettenburg, H. I. C. Dalgarno, J. Nylk, C. Coll-Lladó, D. E. K. Ferrier, T. Čižmár, F. J. Gunn-Moore, and K. Dholakia, "Light-sheet microscopy using an Airy beam." Nat. Methods **11**, 541–544 (2014).
10. G. A. Siviloglou, J. Broky, A. Dogariu, and D. N. Christodoulides, "Observation of accelerating Airy beams," Phys. Rev. Lett. **99**, 213901 (2007).
11. J. Baumgartl, M. Mazilu, and K. Dholakia, "Optically mediated particle clearing using Airy wavepackets," Nat. Photon. **2**, 675–678 (2008).
12. P. Polynkin, M. Kolesik, J. V. Moloney, G. A. Siviloglou, and D. N. Christodoulides, "Curved plasma channel generation using ultraintense Airy beams," Science **324**(5924), 229–232 (2009).
13. P. Polynkin, M. Kolesik, and J. Moloney, "Filamentation of femtosecond laser Airy beams in water," Phys. Rev. Lett. **103**, 123902 (2009).
14. D. G. Papazoglou, S. Suntsov, D. Abdollahpour, and S. Tzortzakis, "Tunable intense Airy beams and tailored femtosecond laser filaments," Phys. Rev. A **81**, 061807 (2010).
15. L. Gao, L. Shao, B.-C. Chen, and E. Betzig, "3D live fluorescence imaging of cellular dynamics using Bessel beam plane illumination microscopy," Nat. Protoc. **9**, 1083–1101 (2014).
16. P. G. Pitrone, J. Schindelin, L. Stuyvenberg, S. Preibisch, M. Weber, K. W. Eliceiri, J. Huisken, and P. Tomancak, "OpenSPIM: an open-access light-sheet microscopy platform," Nat. Methods **10**, 598–599 (2013).
17. J. Wang, J. Bu, M. Wang, Y. Yang, and X. Yuan, "Generation of high quality airy beams with blazed micro-optical cubic phase plates," Appl. Opt. **50**(36), 6627–6631 (2011).
18. W. Chi and N. George, "Electronic imaging using a logarithmic asphere," Opt. Lett. **26**(12), 875–877 (2001).
19. S. Mezouari and A. R. Harvey, "Phase pupil functions for reduction of defocus and spherical aberrations," Opt. Lett. **28**(10), 771–773 (2003).
20. S. Mezouari, G. Muyo, and A. R. Harvey, "Circularly symmetric phase filters for control of primary third-order aberrations: coma and astigmatism," J. Opt. Soc. Am. A **23**(5), 1058–1062 (2006).
21. H. Zhao, Q. Li, and H. Feng, "Improved logarithmic phase mask to extend the depth of field of an incoherent imaging system," Opt. Lett. **33**(11), 1171–1173 (2008).
22. J. Broky, G. A. Siviloglou, A. Dogariu, and D. N. Christodoulides, "Self-healing properties of optical Airy beams." Opt. Express **16**(17), 12880–12891 (2008).
23. P. J. Keller, A. D. Schmidt, J. Wittbrodt, and E. H. K. Stelzer, "Reconstruction of zebrafish early embryonic development by scanned light sheet microscopy," Science **322**(5904), 1065–1069 (2008).
24. R. C. Gonzalez and R. E. Woods, *Digital Image Processing*, 3rd ed. (Prentice Hall, 2007).

1. Introduction

Since the concept of light-sheet imaging was re-visited ten years ago [1], light sheet fluorescence microscopy (LSFM) is becoming increasingly important in biological research, in particular for monitoring the development of large three-dimensional samples. In LSFM, only a thin layer of the sample is illuminated at a time and the images are captured perpendicular to the illuminated plane. Such optical sectioning ability enables high-contrast, high axial resolution whilst minimizing sample exposure and thus phototoxicity.

The axial resolution of light sheet microscopy is determined by the combination of the numerical aperture (NA) of the detection objective and the thickness of the light sheet [2]. For Gaussian-beam illumination, a large field of view (FOV) requires a relatively thick light sheet, thus compromising axial resolution or exposing the sample unnecessarily to excess irradiation. Dual-side illumination [3, 4] or moving the sample along the illumination plane [5] can extend the FOV; however, both methods increase the sample irradiation and may thus induce more photo-bleaching and photo-damage. High axial resolution over an extended FOV has been achieved by digitally scanning a propagation-invariant Bessel or Airy beam [6–9]. Compared to Gaussian beams, propagation-invariant beams such as Bessel or Airy beams maintain their beam profile over a larger distance, hence a uniformly thin light sheet can be created over a larger FOV. In particular we have recently shown the advantages of using the Airy light field

#214434 - $15.00 USD Received 24 Jun 2014; revised 18 Aug 2014; accepted 22 Aug 2014; published 5 Sep 2014

over either the Gaussian or Bessel field in single-photon light-sheet imaging [9].

A conventional, Gaussian, light sheet can be created by either digitally scanning a focused Gaussian laser beam into a homogeneous sheet or by using a cylindrical lens for the same purpose. The former approach offers greater control over the size, homogeneity, and shape of the light sheet, while the latter allows for a compact and low-cost implementation. We show that, in contrast to the Bessel beam, the Airy beam does not need to be scanned to create the light sheet, a cylindrical lens produces the same time-averaged intensity distribution. This enables a significant reduction in size and complexity of the optics.

An Airy beam can be generated through the Fourier transformation of a cubic phase imposed upon an incident Gaussian beam [10, 11]. This typically involves the use of a (liquid crystal) spatial light modulator (SLM) or custom designed cubic phase mask [12, 13]. Neither is readily available nor inexpensive. We therefore aim to use only the components present in a standard light-sheet microscope setup. Typically the misalignment of optical elements is avoided as it induces optical aberrations that degrade image quality and reduce efficiency; however, as we demonstrate here, controlled tilting of the cylindrical lens can induce aberrations that closely approximate the cubic modulation required for Airy light sheet microscopy [14].

The practical applications of advanced light-sheet microscopy are often limited by the high cost and complexity of its implementation. A recent protocol has provided useful information to develop a Bessel-mode light-sheet microscope [15], however such systems still pose a significant level of complexity for non-experts. We based our experimental implementation of an Airy light-sheet system on OpenSPIM, an open-access platform that provides a step-by-step guide to building a compact light-sheet microscope with a Gaussian focus [16]. Only minor modifications were required to add Airy functionality to this compact and low-cost light-sheet microscope. Before experimentally demonstrating this concept, we explored its potential and evaluated its performance using simulations with optical design software `Zemax`.

The following section introduces the theoretical concepts. Prior to the experimental implementation, the expected performance was analyzed. This is discussed in section 3, supported by detailed simulations of the optical model. Section 4 describes the experimental implementation and discusses the results.

2. Theoretical concepts and performance

The two-dimensional Airy beam has a theoretical intensity distribution proportional to $\mathrm{Ai}(sx)^2 \cdot \mathrm{Ai}(sy)^2$, where $\mathrm{Ai}(x)$ and $\mathrm{Ai}(y)$ are the Airy function along the x and y axes respectively, and s is a scale factor. Upon propagation, this asymmetric intensity distribution translates transversely but does not change otherwise. When a light sheet is formed by scanning such a beam along the y-dimension, its intensity cross section will be proportional to a one dimension squared Airy function: $\mathrm{Ai}(sx)^2$.

In practice, specialized beams are often generated in the focal region of a microscope objective by modulating the field at its back aperture with a complex function, $\mathrm{P}(u,v)$, of the pupil coordinates u and v. The two-dimensional Airy beam can be created by introducing a polynomial cubic phase modulation [10, 17]:

$$\begin{aligned} \mathrm{P}(u,v) &= \exp(2\pi \mathrm{i}\ \alpha(u^3+v^3)) \\ &= \exp(2\pi \mathrm{i}\ \alpha u^3)\cdot\exp(2\pi \mathrm{i}\ \alpha v^3), \end{aligned} \tag{1}$$

where the dimensionless parameter α controls the propagation invariance of the Airy beam and the axial contrast of the images [9]. Typical values of α are between 2 and 10 for light sheet imaging, corresponding to the maximum phase modulation in units of wavelength at the edge of the aperture [9].

#214434 - $15.00 USD Received 24 Jun 2014; revised 18 Aug 2014; accepted 22 Aug 2014; published 5 Sep 2014

When only a horizontal line $v \equiv 0$ of the back aperture is illuminated by a cylindrical lens, a light sheet is formed in sample space orthogonal to this axis. The intensity cross section of this light sheet can be determined from the squared Fourier transform of the one-dimensional function $\exp(2\pi i\, \alpha u^3)$ and is proportional to $\mathrm{Ai}(sx)^2$. An Airy light sheet can thus be created using a cylindrical lens as well as by using digital scanning.

A one-dimensional Airy beam may be generated using a combination of two carefully misaligned cylindrical lenses that induce coma aberration with a cubic phase profile across the beam [14]. The Seidel aberration in a single spherical lens takes the form

$$\phi^{(4)}(\rho,\theta,h_0) = Bh_0^3\rho\cos\theta - \frac{1}{2}(2C\cos^2\theta + D)h_0^2\rho^2 + Eh_0\rho^3\cos\theta - \frac{1}{4}F\rho^4 \qquad (2)$$

where B, C, D, E, and F are the distortion, astigmatism, field curvature, coma aberration and spherical aberration coefficients, respectively; h_0 is the object height; ρ is the pupil radius; and θ is the polar angle at the exit pupil of the lens. It is clear that for $\theta = 0$ the cubic functions of ρ will lead to a spatial cubic phase modulation on the output wavefront, which can be achieved by changing the object height with respect to the cylindrical lens, or thus tilting the lens. Unfortunately, quadratic-and higher-order terms are produced along with the cubic term. In the two-cylindrical-lens optical system in [14], one lens creates a high-order one-dimensional (1D) polynomial phase profile and the other lens creates a phase profile that minimizes all but the third-order terms, making the cubic phase profile dominant. The output of this two-lens arrangement is a collimated beam with 1D cubic phase modulation. To further make a light sheet from this optical system requires an additional cylindrical lens, adding size and complexity to the optical system.

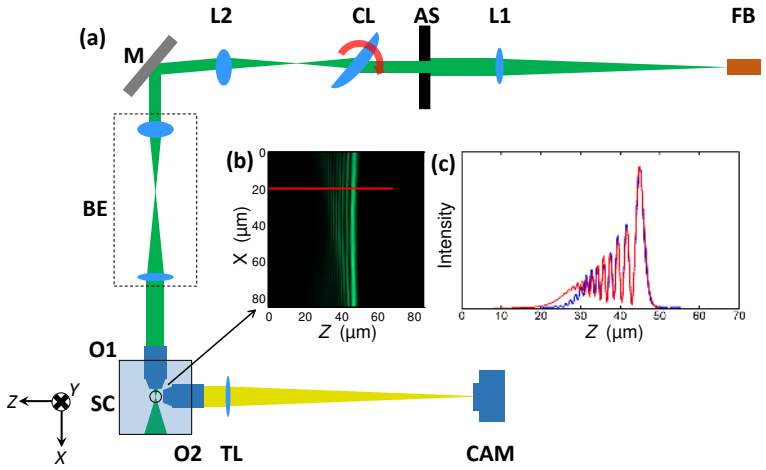

Fig. 1. Schematic of the open-access Airy light-sheet microscope. (a) Experimental setup with tilted cylindrical lens (CL). (b) shows the projection of measured Airy light sheet. (c) The red line shows the beam profile of a cross section on (b). The blue line indicates the corresponding Airy beam profile from fitted model.

As such, we created an Airy light sheet with only two optical elements by: tilting the cylindrical lens used in OpenSPIM microscope design (CL, Fig. 1) to introduce coma aberration, and placing a re-collimating lens (L2, Fig. 1) between the cylindrical lens and the proceeding telescope which is also a beam expander (BE, Fig. 1). The spherical re-collimating lens (L2) performs the role of the aberration compensating cylindrical lens (as used in [14]), as well as

#214434 - $15.00 USD Received 24 Jun 2014; revised 18 Aug 2014; accepted 22 Aug 2014; published 5 Sep 2014

that of the additional cylindrical lens required for light sheet formation. The first order term in the aberration is absent when tilting the cylindrical lens around the center of its convex front surface; however, a lateral displacement of the optical axis cannot be avoided. We compensate for this displacement by adjusting a mirror after the re-collimating lens (M and L2 in Fig. 1, respectively). The second order polynomial component can be seen as a one-dimensional defocus, which in the case of light sheet illumination can be readily compensated for by adjustment of the short-focal-length lens (L2, Fig. 1). This lens changes the orientation of the light sheet, hence the cylindrical lens was rotated 90° around the propagation axis to bring the light sheet back to the correct orientation.

The presence of higher order terms such as spherical aberration and higher order coma will be detrimental to the Airy light sheet quality. Note however that this does not necessarily prevent high resolution imaging. In fact, the introduction of various higher-order aberrations has proven useful for imaging in the presence of aberrations [18–21]. Residual higher order terms may thus be of less importance to the final image quality, though the microscope may require additional calibration before use. We thus investigate any deviation from the cubic modulation in what follows.

3. Simulations

The impact of the tilt-angle of the cylindrical lens (LJ1695RM-A, Thorlabs) with focal length (FL) 50 mm, is assessed using the accompanying `Zemax` model for various system parameters. Due to the symmetry in the optical system, a one-dimensional array of rays is sufficient to characterize the optics. An array of 100 rays, uniformly spaced over a distance of 5 mm is traced through the center of the convex front surface of the tilted cylindrical lens. The optical path lengths of each ray are determined at the focal point, defined as the point where the standard deviation in optical path length is minimal. A cubic polynomial is fitted to determine the α-value, and the residual is determined to assess the presence of higher order terms. This process is repeated for 121 cylindrical lens tilt angles between 0 and 60° and for five typical excitation laser wavelengths.

As can be seen from Fig. 2(a) and (b), the position of the focal point is clearly dependent on the lens angle. Adjusting the modulation will thus require readjusting the position of the cylindrical lens; however, minimal wavelength dependency is seen (Fig. 2(a) and (b)), even if the cylindrical lens is a singlet lens.

The cubic modulation varies dramatically for lens angles between 0 and 60° (Fig. 2(c)). Tilt angles between 40° and 45° result in cubic polynomial coefficients in the range typically required for Airy light sheet microscopy [9]. The residual modulation is calculated as the root-mean-square optical path difference after subtracting the cubic term. It can be seen to increase rapidly for angles close to 60°; however, between 40° and 45° it is negligible ($< \lambda/10$, Fig. 2(d)). In this range, the focal position varies only by a few millimeters (Fig. 2(a) and (b)).

As the cylindrical lens we employ is not an achromat it should be of no surprise that some wavelength dependency is present in the phase modulation. The cylindrical lens position and tilt angle may have to be adjusted when changing laser source. Here we choose a tilt angle of 40° for an excitation wavelength of 532 nm in our experimental setup. This should provide a theoretical cubic modulation of approximately $\alpha = 4.13$.

4. Experimental validation

A light sheet microscope, based on the OpenSPIM design, was constructed as shown in Fig. 1. Laser (Verdi V6, 6 W, 532 nm, Coherent) is introduced with a single-mode fiber (FB) and then collimated by lens L1 (LA1708-A-ML, FL 200 mm, Thorlabs). An adjustable slit AS (VA100/M, Thorlabs) varies the width of incoming beam, allowing us to control the NA of

#214434 - $15.00 USD Received 24 Jun 2014; revised 18 Aug 2014; accepted 22 Aug 2014; published 5 Sep 2014

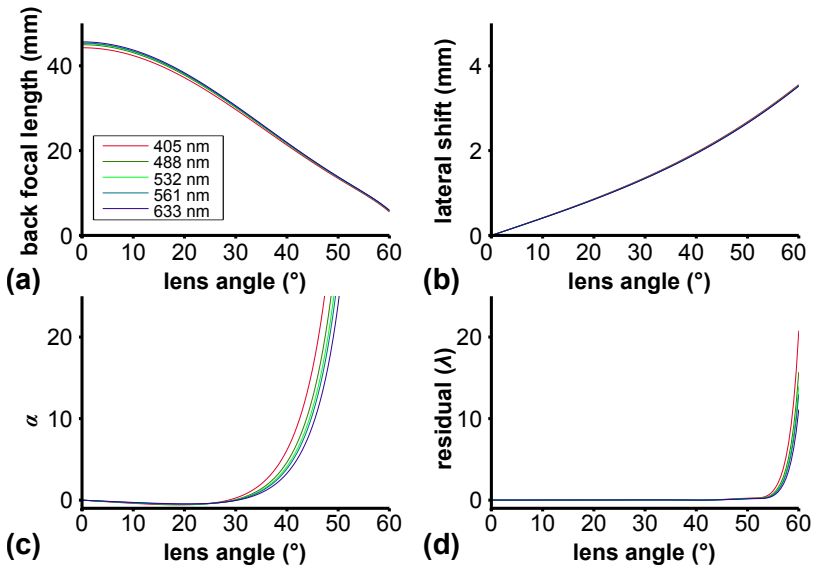

Fig. 2. Influence of the cylindrical lens tilt angle. (a) focal length, (b) optical axis displacement, (c) cubic and, (d) higher order modulation residual, as a function of the lens angle. The line colors correspond to the wavelengths 405 nm, 488 nm, 532 nm, 561 nm, and 633 nm. At the wavelength of 532 nm used in the experiments, the α value is 1.21 at 35°, 4.13 at 40°, and 11.24 at 45°, covering the values useful for Airy beam light sheet microscopy. Almost no higher order terms are present as can be seen from (d). The residual phase modulation has a standard deviation of only $0.026\,\lambda$, $0.006\,\lambda$, and $0.061\,\lambda$, respectively. The corresponding focal lengths are 26 mm, 22 mm, and 18 mm. The axis position shifts by 1.6 mm, 1.9 mm, and, 2.3 mm. The focus position at a wavelength of 488 nm differs by less than 1%. As a result, the optics do not need to be adjusted for minor changes in wavelength.

the illumination. A tilted and shifted cylindrical lens (CL, LJ1695RM-A, FL 50 mm, Thorlabs) introduces coma aberration and creates the 1D Airy light sheet. Minimization of other aberrations is achieved with the short-focal-length lens (L2, AC127-025-A-ML, FL 25 mm, Thorlabs) and the steering mirror (M). The focal length of L2 was chosen to closely match the back focal length of CL at the tilt angle used (see Fig. 2(a)) to avoid changing the diameter of the beam. The light sheet is imaged into the sample chamber (SC) by the lens L2, a beam expander (BE, 2×) and the illumination objective (O1, UMPLFLN 10×W, 10× water dipping, NA 0.3, Olympus). Images are acquired perpendicular to the illumination plane with another objective (O2, CFI Apo 40×W NIR, 40× water dipping, NA 0.8, Nikon), a tube lens (TL, LA1708-A-ML, FL 200 mm, Thorlabs) and a camera (CAM, CCD, piA640-210gm, Basler). The whole setup fits well within the space of 35cm × 35cm × 10cm on a breadboard, including the XYZ translation stage for mounting the sample (beside the sample chamber and not shown in Fig. 1). By changing the existing translation stage to a more compact automatic stage, the physical dimensions of the system can be further reduced, emphasizing its potential as a portable system.

In an initial phase we determine the three-dimensional intensity distribution of the light sheet. This is achieved by translating a small mirror in the sample chamber and recording the reflection plane-by-plane. The reconstructed beam profile along the axis is shown in Fig. 1(b). Next, a model of the light sheet is fitted to the measurement. We considered phase modulations up to fifth order and, to account for non-uniform illumination of the back aperture, amplitude

#214434 - $15.00 USD Received 24 Jun 2014; revised 18 Aug 2014; accepted 22 Aug 2014; published 5 Sep 2014

modulation up to third order polynomials. The experimentally measured light sheet deviated significantly from its theoretical prediction. The cubic modulation was found to be higher $\alpha = 7.8$, while four and fifth order components were present, 1.65 and -2.9, respectively. Also the illumination was not uniform, with normalized linear, quadratic, and cubic components of 0.6, -0.5, and 0.4, respectively. Figure 1(c) shows the comparison between the recorded beam profile (red line) and the fitted model (blue line). We attribute this discrepancy with the theoretical model to minor misalignments in the optics. However, we found that the fitted model allowed accurate decon volution of the recorded data.

Although a cylindrical lens is straightforward to use and cost effective, it does reduce the uniformity of the Gaussian light sheet and may also affect the Airy light sheet to some extent, even if the propagation of the Airy beam has been reported to be more robust to optical inhomogeneities in its path [22]. Although we found the light sheet uniformity to be sufficient for deconvolution, more demanding samples may require the addition of a scanning mirror to improve the uniformity [23]. However, the cylindrical lens can still be used to create the Airy profile.

We tested the system by recording three-dimensional data-stacks of red fluorescent microspheres (R600, Thermo Scientific, $\varnothing = 600\,\text{nm}$) embedded in 1.5% agarose and suspended in the water-immersed sample chamber from above. The suspended sample was scanned using a motorized actuator (CMA-25CCCL, Newport) on a XYZ linear stage (M-562-XYZ, Newport) and images were acquired every 185 nm. The vertical projection in Fig. 3(a) clearly shows how the asymmetric transversal structure of the Airy light sheet interacts with each microsphere to create an axially elongated tail. For this experiment, the NA of the detection objective was reduced with an iris to increase the depth of field of the detection objective and accurately capture this pattern. Care was taken to align the stage movement with the optical axis of the detection objective; however, a small deviation was still detected in the elongated tails. The residual error was found to be consistent and thus corrected by digitally warping the recorded data by a small amount before applying the deconvolution [9, 24].

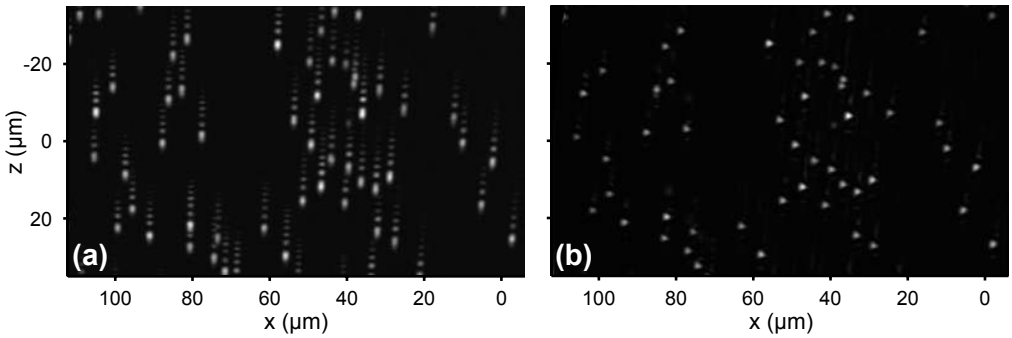

Fig. 3. Vertical projection of a sample with fluorescent microspheres ($\varnothing = 600\,\text{nm}$), before deconvolution (a), and after deconvolution (b). Although before deconvolution the fluorescent microspheres appear blurred in the axial dimension, z, the pattern is relatively independent of the horizontal coordinate, x. Deconvolution using the light sheet model yields comparable resolution throughout the FOV.

Figure 3(b) shows that the axial resolution across the FOV. The axial resolution was measured to be consistently 1.9 μm across the entire FOV of the camera sensor chip (CCD, piA640-210gm, Basler). A Gaussian light sheet with equivalent NA would provide axial resolution of 1.4 μm and only remain confined in the Rayleigh interval $-4\,\mu\text{m} < x < 4\,\mu\text{m}$, accurate deconvolution may be possible over a larger FOV ($-25\,\mu\text{m} < x < 25\,\mu\text{m}$) [9]. In contrast, the

#214434 - $15.00 USD Received 24 Jun 2014; revised 18 Aug 2014; accepted 22 Aug 2014; published 5 Sep 2014

Airy light sheet illumination gives access to areas that are at least four times more distant from the light sheet waist, essentially enabling high axial resolution across the sensor area. With further optimization we believe we can attain up to a ten-fold improvement over the Gaussian beam as shown in our previous work using a sophisticated SLM setup [9].

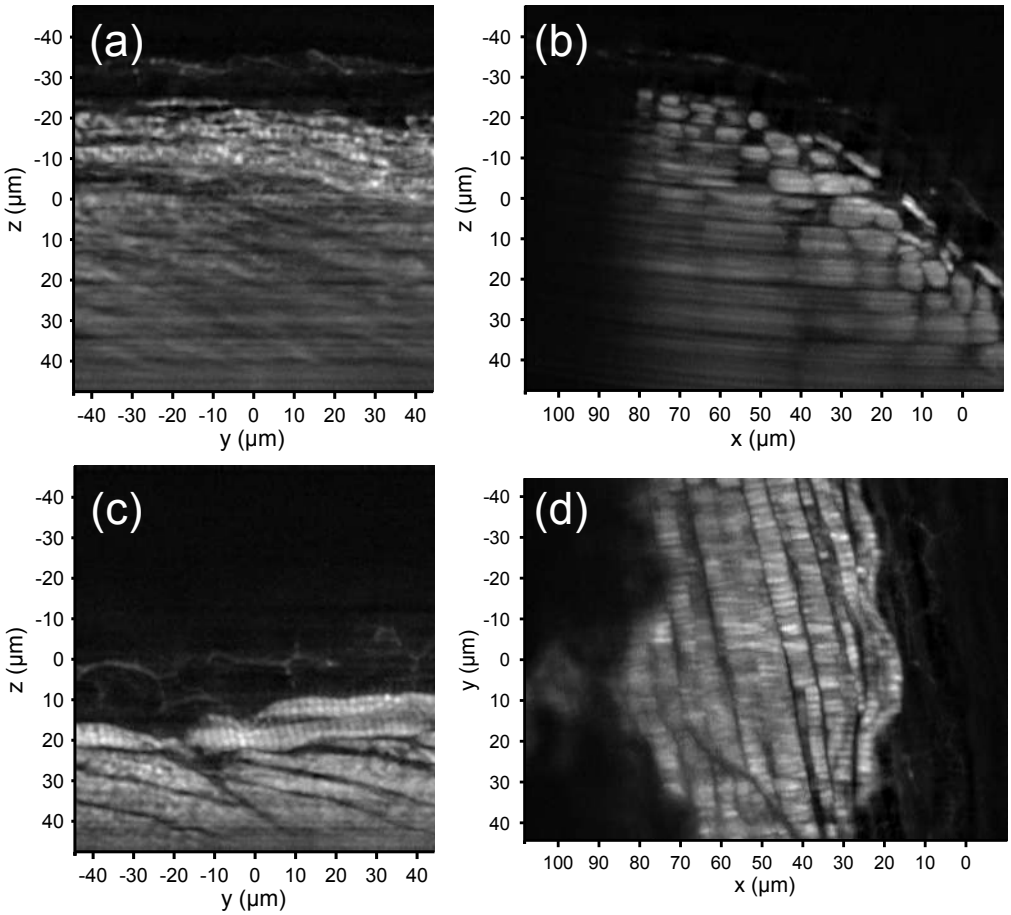

Fig. 4. Light-sheet microscopy scan of the musculature of a zebrafish larva. Two distant sections along the light sheet propagation axis (x) are shown at $x = +45$ μm (a) and $x = -10$ μm (c). Two-dimensional sections are shown at $y = -40$ μm (b) and at $z = -10$ μm (d). The thickness of each section is 7.4 μm. The transverse view of the musculature (b) shows the diameter of individual muscle fibers, which vary in size. In the longitudinal views of the musculature (c, d), a fragment of the V-shaped myosepta separating two muscle blocks can be appreciated: in (c) the myosepta (dark diagonal line) extends from ($y = -20$ μm, $z = 20$ μm) to ($y = 10$ μm, $z = 50$ μm), and in (d) extends from ($x = 70$ μm, $z = 15$ μm) to ($x = 40$ μm, $z = 45$ μm).

As an example of a large, highly scattering sample, we imaged musculature in a zebrafish larva, see Fig. 4. At 14 days post fertilization (14-dpf), the zebrafish larva (*Danio rerio*, gender not determinable at age) was humanely killed by an overdose of tricaine methane sulfonate (MS-222, Sigma). Schedule 1 techniques were used in compliance with the Animals (Scientific Procedures) Act regulations and are authorized by the Animal Welfare and Ethics Committee of the University of St Andrews. The zebrafish larva was then fixed in 4% (w/v) paraformalde-

#214434 - $15.00 USD Received 24 Jun 2014; revised 18 Aug 2014; accepted 22 Aug 2014; published 5 Sep 2014

hyde (PFA) in PBS (1× phosphate buffered saline solution) overnight at 4°C without agitation. The tissue was subsequently permeabilized by washing it three times in PBT (1× PBS, 0.1% Triton X-100). Muscle fibers were visualized by staining actin filaments with Alexa Fluor 555 phalloidin (Life Technologies), the zebrafish larva was stained overnight at 4°C in continuous agitation, with Alexa Fluor 555 phalloidin diluted 1:100 (v/v) in PBT. The zebrafish was then rinsed three times in PBT and embedded in 1.5% low melting point agarose.

5. Conclusion

We have demonstrated a low-cost compact Airy-beam light-sheet microscope, constructed by converting a conventional light sheet microscope using readily-available, off-the-shelf optical components. The entire optical setup fits well within the small footprint of 35 cm × 35 cm × 10 cm. This size can be further reduced by exchanging the existing stage for a more compact one and fitting it in the center of the setup as in [16]. The compactness and portability of the system is essential to make this technology more accessible to biologists and brings more opportunities for advanced biomedical applications. Simulations showed that tilting the cylindrical lens allowed a controllable amount of cubic phase modulation in order to generate the Airy light sheet, while the additional tilt and defocus are readily compensated for by appropriate use of relay optics. Our experimental images of embedded fluorescent microspheres and zebrafish larva muscle tissue show that the axial resolution is comparable to that expected from a Gaussian light sheet, yet across the full FOV of the detector area. This proof-of-principle implementation demonstrates that the advantages of beam-shaping can be readily exploited for advanced light sheet microscopy with a wide range of biomedical endusers.

Acknowledgments

We thank the UK Engineering and Physical Sciences Research Council under grant EP/J01771X/1, the 'BRAINS' 600th anniversary appeal and Dr. E. Killick for funding.

#214434 - $15.00 USD Received 24 Jun 2014; revised 18 Aug 2014; accepted 22 Aug 2014; published 5 Sep 2014